

## Potential increase in floods in California's Sierra Nevada under future climate projections

Tapash Das · Michael D. Dettinger · Daniel R. Cayan ·  
Hugo G. Hidalgo

Received: 9 March 2010 / Accepted: 17 June 2011 / Published online: 24 November 2011  
© Springer Science+Business Media B.V. 2011

**Abstract** California's mountainous topography, exposure to occasional heavily moisture-laden storm systems, and varied communities and infrastructures in low lying areas make it highly vulnerable to floods. An important question facing the state—in terms of protecting the public and formulating water management responses to climate change—is “how might future climate changes affect flood characteristics in California?” To help address this, we simulate floods on the western slopes of the Sierra Nevada Mountains, the state's primary catchment, based on downscaled daily precipitation and temperature projections from three General Circulation Models (GCMs). These climate projections are fed into the Variable Infiltration Capacity (VIC) hydrologic model, and the VIC-simulated streamflows and hydrologic conditions, from historical and from projected climate change runs, allow us to evaluate possible changes in annual maximum 3-day flood magnitudes and frequencies of floods. By the end of the 21st Century, all projections yield larger-than-historical floods, for both the Northern Sierra Nevada (NSN) and for the Southern Sierra Nevada (SSN). The increases in flood magnitude are statistically significant (at  $p \leq 0.01$ ) for all the three GCMs in the period 2051–2099. The frequency of flood events above selected historical thresholds also increases under projections from CNRM CM3 and NCAR PCM1 climate models, while under the third scenario, GFDL CM2.1, frequencies remain constant or decline slightly, owing to an overall drying trend.

---

T. Das (✉) · M. D. Dettinger · D. R. Cayan  
Division of Climate, Atmospheric Sciences, and Physical Oceanography, Scripps Institution of  
Oceanography, University of California San Diego, Mail Code 0224, La Jolla, CA 92093-0224, USA  
e-mail: tapash.das@ch2m.com

M. D. Dettinger · D. R. Cayan  
United States Geological Survey, La Jolla, CA, USA

H. G. Hidalgo  
School of Physics and Center for Geophysical Research, University of Costa Rica, San Jose, Costa Rica

T. Das  
CH2MHILL, Inc., San Diego, CA 92101, USA

These increases appear to derive jointly from increases in heavy precipitation amount, storm frequencies, and days with more precipitation falling as rain and less as snow. Increases in antecedent winter soil moisture also play a role in some areas. Thus, a complex, as-yet unpredictable interplay of several different climatic influences threatens to cause increased flood hazards in California's complex western Sierra landscapes.

## 1 Introduction

Floods cause immense damage to human societies globally and are thought to be the costliest type of natural disaster in economic and human terms. For example, in United States (US) the total estimated fiscal year 2003 flood damage was almost \$2.5 billion (Pielke et al. 2002). Flood damage fluctuates from year to year, but Pielke and Downton (2000) present an increasing trend in US flood damage over the past century.

Floods are particularly dangerous in California, where topography, exposure to heavy moisture-laden storm systems, and extensive human development and infrastructure in low lying areas add to the risks. In California, most of the large historical floods have arisen from two general mechanisms: (i) winter general floods covering large areas and (ii) spring and early summer snowmelt floods, mostly from the higher elevations of the central and southern Sierra Nevada (Roos 1997). The largest winter floods have historically been most catastrophic and have caused billions of dollars in damages (Roos 1997). Floods in California are linked to winter-spring atmospheric circulations (Cayan and Riddle 1992), with the largest floods most often associated with atmospheric rivers (Ralph et al. 2006; Neiman et al. 2008). These influences, and hence the floods they produce, may be amplified in coming decades as climate becomes warmer, as projected by almost all global climate models.

California is currently faced by many urgent issues concerning floods and will need to make decisions in the context of possible climate changes. For example, the State's long history of major floods, together with ongoing tightening of water-supply options in the State, have led the California Water Plan Update in 2005 to identify integrated flood management actions as a crucial part of improved water supply management DWR (2005a). Such integration must address inherent and longstanding conflicts between management of California's reservoirs for flood protection versus their management for dry-season water supplies. But even as flood flows are accepted as a component of future water-supply solutions for the state, the recognized potential for flood-induced failures of aging levee systems, for widespread flood damages, and for disruptions of freshwater conveyances throughout the Central Valley, and especially in the Sacramento-San Joaquin Delta, threatens the State's communities and infrastructures, as well as its largest scale water-supply conveyances. Furthermore, there is a growing understanding that floods and floodplains play fundamental roles in the sustainability of Delta and Central Valley ecosystems and water quality (Healey et al. 2008). In addressing these pressing challenges, informed decisions now require greater understanding and, eventually, reliable projections of future flood responses to likely 21st Century climate changes. That understanding and those projections are still very much matters of research, of which the present study is an early example.

Long-term changes in hydro-meteorological variables have already been documented across the western US, including large increases in winter and spring temperatures (e.g., Dettinger and Cayan 1995; Bonfils et al. 2008), substantial declines in the volumes of snow pack in low and middle latitudes (Lettenmaier and Gan 1990; Knowles and Cayan 2004), significant declines in April 1st snow water equivalent (SWE) (Mote et al. 2005; Pierce et al. 2008), shifts toward more rainfall and less snowfall (Knowles et al. 2006), earlier streamflow in snowfed rivers (Dettinger and Cayan 1995; Cayan et al. 2001; Stewart et al. 2005), and sizeable increases in

winter streamflows as fractions of water-year totals (Dettinger and Cayan 1995; Stewart et al. 2005). Recently Barnett et al. (2008) performed a formal multivariate detection and attribution study and showed that observed changes in the mountainous regions of the western US of minimum temperature, SWE as a fraction of precipitation, and center timing of streamflow covary during the period 1950–1999. They concluded, with a high statistical confidence, that up to 60% of the observed trends in those variables have been driven by increasing greenhouse effects and attendant temperature increases. In response to projected continuing increases in greenhouse-gas emissions, current climate change projections by the end of the 21st century California uniformly yield warming by at least a couple of degrees Celsius, and, although great uncertainties exist about future changes in long-term average precipitation rates in California (e.g., Dettinger 2005; Cayan et al. 2008a,b), it is generally expected that extreme precipitation episodes will become more extreme as the climate changes (Easterling et al. 2000).

Many studies have been performed to investigate the potential impact of these kinds of climate changes on California's hydrology at seasonal and longer time scales (for example, see Lettenmaier and Gan 1990; Miller et al. 2003; Knowles and Cayan 2004; Dettinger et al. 2004; Maurer 2007; Cayan et al. 2008a; Cayan et al. 2010), finding changes in streamflow timing, warm season vs. cool season runoff, low flow season discharges, and overall flow totals. Given all of the observed and predicted hydrologic changes across the western US, it is reasonable to wonder whether there may be changes in the frequencies and magnitudes of floods as well. Projected climate changes may affect California's flood magnitudes and frequencies, and even the mechanisms by which floods are unleashed, in a variety of ways. Tendencies towards larger storm precipitation totals or more frequent large storms, or the reverse, could directly change the opportunities for floods. Projected warming trends would continue or increase recent trends toward having more precipitation fall as rain and less as snow (Knowles et al. 2006; Das et al. 2009), which could affect both magnitudes and frequencies of floods by increasing the catchment areas from which precipitation (rain) runs off most rapidly or by increasing the frequency of storms with large rainfall runoff totals. Warming may also change catchment water balances to alter antecedent hydrologic conditions that set the stage for floods, e.g., by increasing rates and opportunities for evapotranspiration to sap soil-moisture reservoirs.

In California, the magnitude of 100-year floods estimated from the early historical period was smaller than recently observed floods, suggesting either that the records used to estimate 100-year floods was too short or subject to recent changes in climate (Anderson et al. 2006; DWR 2005a, b; 2007). Dettinger et al. (2004) evaluated future flood risks in specific California basins and found increased risks from warming alone. Miller et al. (2003) found increased likelihood of more floods in California under climate change. Hamlet and Lettenmaier (2007) identified increased flood risk tendencies in warmer basins along the coasts of Washington, Oregon and California using 20th century precipitation and temperature in a hydrological model. Milly et al. (2008) argued "now is an opportune moment to update the analytic strategies used for planning such grand investments under an uncertain and changing climate." More recently, Dettinger et al. (2009) and Raff et al. (2009) predicted general increases in flood magnitude with climate change.

Although uncertainties abound, planning and investments for flood management in California must somehow accommodate potentially changing flood challenges due to climate changes. The projected climate changes may affect California's flood regimes in several ways, such as (Dettinger et al. 2009):

- Potential to intensify or ameliorate of flood magnitudes
- Potential for increase, or decrease, frequencies of floods
- Potential for changing seasonalities and mechanisms of floods

In each case, such changes will remain uncertain. For example, arguments can be made that, with more water vapor and heat in the atmosphere, storms and thus floods should become more intense (e.g., Trenberth 1999) or larger overall; however, as the polar regions warm more quickly than the lower latitudes, the equator-to-pole temperature differences are expected to decrease (Jain et al. 1999) which generally would be expected—from basic geophysical fluid dynamics considerations—to weaken mid latitude storm tracks. Which change will dominate California's future flood regimes? Because the humid tropics have the strongest greenhouse effect, more heat will need to be transported poleward as the world warms and thus mid latitude storms (an important mechanism for poleward heat transport) may become more frequent. Alternatively, declining equator-to-pole temperature differences might tend to weaken storm tracks and reduce storm frequencies. Even with weakening storm tracks, however, trends towards warmer storms may result in more precipitation as rain rather than snow (Knowles et al. 2006; Das et al. 2009), changing the mechanisms and opportunities for flood generation in California's higher and wetter catchments to increase the percentage of storms that generate floods. In such a case, would weakening storm tracks or increasing rain fractions dominate to decrease or increase the numbers of overall floods? In a warming region, with presumed increases in the demands and opportunities for evaporation and transpiration, soils are likely to generally be drier (unless total precipitation increases considerably), which could reduce risks of floods. Alternatively, though, as long as some snow is still being deposited in the state, it is likely that warmer winters—at least—may induce more mid-winter snowmelt and thus wetter soils in winter, which might make flooding more likely. Thus future flood regimes are likely to depend on delicate and difficult balancing between several different kinds of climate-change effects and hydrologic responses. An integrated, hydrologic modeling approach is thus required to assess the net or overall flood-regime changes that might result.

The present study simulates possible changes in annual maximum 3-day flood magnitudes and frequencies for floods exceeding selected historical thresholds under a range of projected climate changes. Potential flood conditions were simulated by forcing the Variable Infiltration Capacity (VIC) hydrologic model with downscaled daily precipitation and temperature projections from three General Circulation Models (GCMs) (CNRM CM3, GFDL CM2.1 and NCAR PCM1). Further analysis was performed to examine possible mechanisms with the associated flood regime change.

This article is organized as follows. Section 2 presents data sets and models used in our study. A description of the method is given in Section 3. Section 4 presents model results and possible mechanisms for the projected flood regime changes. A summary and conclusions are given in Section 5.

## 2 Datasets and models

### 2.1 Observed meteorology

Daily observations of precipitation (P), maximum daily temperature (Tmax), minimum temperature (Tmin), and wind speed gridded to 1/8° spatial resolution across California were obtained from the Surface Water Modeling Group at the University of Washington (<http://www.hydro.washington.edu>; Hamlet and Lettenmaier 2005). The data are based on the National Weather Service co-operative network of weather observations stations, augmented by information from the higher quality Global Historical Climatology Network (GHCN) stations. The dataset also relies on monthly PRISM data fields (Daly et al. 1994)

to adjust for elevation effects on precipitation and temperature. Such corrections are necessary because topography in the study region strongly determines not only spatial patterns of precipitation (and temperature) but also basin-scale to regional totals of precipitation. The Hamlet and Lettenmaier (2005) dataset is available for the period 1915 through 2003, but hydrologic simulations in this study were of the period 1950–1999.

## 2.2 Global climate models and downscaling

Because global-scale climate models operate on very coarse spatial grids (with grid cell centers separated by 1 to 2° of latitude and longitude or about 100-km to 200-km), the representation of topography and thus of orographic enhancements of precipitation are almost entirely muted (Dettinger et al. 2004; Dettinger 2005; Maurer 2007; Cayan et al. 2008a,b). Downscaling methods are used to obtain local-scale representations of surface weather from the regional-scale atmospheric variables provided by GCMs. Daily P, Tmax and Tmin from three GCMs (CNRM CM3 model, GFDL CM2.1 and NCAR PCM1) were downscaled to 1/8° resolution (about 12-km) using the Constructed Analogues (CA; Hidalgo et al. 2008, 2009; Maurer and Hidalgo 2008) statistical downscaling method. These three GCMs were selected from among the six GCMs used by the California Climate Action Team in its recent California Climate Change Assessment (Cayan et al. 2009; Franco et al. 2011, in this issue). The selection of the global models was guided by several different factors, including having a good representation of typical patterns of El Niño-Southern Oscillation (ENSO) and Pacific Decadal Oscillation (PDO) and realistic representation of mean climate and its decadal variability over California. Another selection criterion was the availability of daily precipitation and temperature data required for the CA downscaling procedure, and to set up a hydrological model to simulate future floods. Flood responses to historical climates, as simulated by each GCM under 20c3m estimates of historical emissions, and to future climates under the medium-high emission scenario (SRES A2; IPCC 2007) are simulated and evaluated here. In the A2 emission scenario, emissions accelerate throughout the 21st Century, and, by the end of the 21st century, atmospheric CO<sub>2</sub> concentrations reach more than triple their pre-industrial levels. This emission scenario yields significant climate change; thus, if climate change could alter flood conditions in California, we expect that evidence will emerge from simulations using this scenario. However, because a broader range of scenarios is not evaluated here, the present results cannot be interpreted as prediction of flood changes but rather as examples of levels of flood change that could plausibly develop in the 21st Century.

In the constructed analogues (CA) method, downscaled climate fields at 1/8° are obtained by constructing linear combinations of previously observed weather patterns, including adjustments for model biases. A library of gridded meteorological observations, based on Maurer et al. (2002) from the period 1950 to 1999, coarsened to match the GCM grid is searched at each GCM time step to locate 30 best analogues of the GCM output for a given day. The 30 previously observed daily patterns most similar (at GCM resolution) to the GCM pattern to be downscaled are then joined by a linear regression to obtain a linear combination that best matches, on the GCM grid, the GCM pattern to be downscaled. Once the best combination of past patterns and the regression-based linear combination of them are obtained, the same linear combination is applied to the original high-resolution Maurer et al. (2002) fields from the same historical days to obtain a high-resolution version of the meteorological conditions corresponding to the daily GCM pattern in question. Downscaling by CA and by the bias correction and spatial downscaling (BCSD), another statistical

downscaling methodology, yield results that are quantitatively similar (Maurer and Hidalgo 2008). An advantage of the CA method over the BCSD method is that CA can capture changes in the diurnal cycles of temperatures and changing weather extremes in the GCM outputs. The original version of the CA method (Hidalgo et al. 2008) does not include as extensive a bias-correction of the GCM data as does BCSD, instead including only the bias-correction that was obtained through working with anomalies of the GCM data. But in this work we add a simple post-downscaled bias-correction for precipitation, as follows. As a first step, for every 12-km VIC gridcell, we compute ratios of long term monthly observed precipitation (Maurer et al. 2002) and long term monthly precipitation of GCM historical simulation (so called 20c3m simulation) for the period 1950–1999, for 12 months. In the second step, these ratios are multiplied by the daily values of downscaled precipitation for the period 1950–2099 (thus using the multiplier factor to the downscaled future precipitation). By doing this, no day-to-day correspondence between the model historical simulation and observations could be expected, however the downscaled mean seasonal cycle of precipitation, at 12-km grid scale, is expected to be much the same as the 50 year observed climatology for downscaled model historical simulations. Interested readers are referred to an investigation of advantages of bias-correction procedures (Maurer et al. 2010a).

### 2.3 Hydrological model

To simulate daily streamflow during the period 1951–1999 and under 21st Century climate change conditions, we used the VIC distributed macro-scale hydrological model (Liang et al. 1994; Cherkauer et al. 2003). Defining characteristics of VIC are the probabilistic treatment of sub-grid soil moisture capacity distribution, the parameterization of baseflow as a nonlinear recession from the lower soil layer, and the unsaturated hydraulic conductivity at each particular time step is treated as a function of the degree of soil saturation (Liang et al. 1994; Maurer et al. 2002). Surface runoff uses an infiltration formulation based on the Xinanjiang model (Wood et al. 1992), while baseflow follows the ARNO model (Todini 1996). It uses a tiled representation of the land surface within each model grid cell, allowing sub-grid variability in topography, infiltration, and land surface vegetation classes (Liang et al. 1994; Maurer et al. 2002). Derived variables such as radiation, humidity and pressure are estimated within the model based on the input  $P$ ,  $T_{\max}$  and  $T_{\min}$  values using the algorithms of Kimball et al. (1997) and Thornton and Running (1999). The calibrated soil parameters for VIC are the same as those used in Barnett et al. (2008) and Hidalgo et al. (2009). The vegetation cover was obtained from the North American Land Data Assimilation System (NLDAS) and was held static through the entire simulation period. The VIC model was run at a daily time step, with a 1-hour snow model time step in water balance mode, and using a  $1/8$  by  $1/8^\circ$  grid resolution. Using the gridded meteorological forcing, along with the physiographic characteristics of the catchment (for example, soil and vegetation properties), VIC calculates a suite of hydrologic variables, including runoff, baseflow, soil moisture, actual evapotranspiration and Snow Water Equivalent (SWE) in the snowpack.

VIC has been used extensively in a variety of water resources applications from studies of climate variability, hydrologic forecasting and climate change studies (for example, Nijssen et al. 2001; Maurer et al. 2002; Sheffield and Wood 2007; Barnett et al. 2008; Wood and Lettenmaier 2006; Dettinger et al. 2011; Cayan et al. 2010). Mote et al. (2005) found reasonable agreement between the spatial pattern of observed SWE and the VIC simulated values. The ability of the model to simulate soil moisture at some of the points is

found satisfactory when compared with the measurements (Maurer et al. 2002). VIC simulated streamflow validates well with observations, for relatively larger catchments at monthly temporal scale when the model has been calibrated using streamflow data (Maurer et al. 2002; Hidalgo et al. 2009). Hamlet and Lettenmaier (2007) performed a study using VIC simulated extreme streamflows to examine flood characteristics across the West (including California), and argued that VIC can be applied to investigate relative changes in flood risks. In the present study, the main focus is to investigate the changes of floods risk under future climate projections.

## 2.4 Study areas

In the present study, flood regimes are analyzed for Northern and Southern parts of the western slopes of the Sierra Nevada (Fig. 1). Drainage areas for the basins simulated here in the Northern Sierra Nevada (NSN) and Southern Sierra Nevada (SSN) are approximately 46,080 km<sup>2</sup> and 15,120 km<sup>2</sup> respectively. Topographic elevation for NSN varies from 150 m (m ASL) to 2480 m, with an average elevation of 1360 m. Annual precipitation spatially varies with topographic structure, from 290 mm to 2050 mm, with an average value of 940 mm. Annual temperature spatially varies from  $-0.3^{\circ}$  C to  $16.4^{\circ}$  C, averaging  $8.1^{\circ}$  C. Topographic elevation for SSN spatially varies from 150 m (m ASL) to 3520 m, with an average elevation of 1840 m. Annual precipitation varies from 345 mm to 1430 mm; with an average value of 990 mm. Annual temperature spatially varies from  $-4.6^{\circ}$  C to  $16.2^{\circ}$  C, averaging  $6.6^{\circ}$  C. Because the NSN area is at lower elevation and warmer, the majority of the streamflow comes directly from winter precipitation and is mixed rain-snow dominated, whereas SSN rivers are dominated by springtime snowmelt runoff (Dettinger et al. 2004).

## 3 Methods

The VIC simulated runoff and baseflow were combined and routed, as in Lohmann et al. (1996), to obtain daily streamflows for locations near the bottom of seven California river basins (Fig. 1). NSN streamflow was computed by adding the routed streamflow from the Sacramento River at Bend Bridge, the Feather River at Oroville and the Yuba River at Smartville. SSN streamflow was obtained by summing daily streamflows from the four main tributaries of the San Joaquin River: the Stanislaus at New Melones Dam, the Tuolumne River at New Don Pedro, the Merced at Lake McClure, and the San Joaquin at Millerton Lake. As stated previously, the main aim is to study possible changes in flood occurrences and flood magnitudes. A historical 99th percentile value of daily streamflow (from November through July) for the period 1951–1999 was obtained from routed flows as simulated with historical meteorology and with the historical simulations from each GCM. These flow values were used as thresholds to define floods for frequency-of-flooding evaluations.

To examine changes in flood magnitudes, we use 3-day maximum annual streamflows simulated by VIC as driven by the downscaled climate model meteorology for the period 1951–2099. The 3-day flood, a measure commonly used for flood planning purposes in California (DWR 2006; Chung et al. 2009), is important because flood-control reservoir space in the Sierra is large enough so that discharge totals over 3 or more days are more representative of uncontrolled flood risks than are shorter term totals. The 3-day peak flow has thus become a standard for climate change impact studies in California (e.g., Brekke et al. 2009; Maurer et al. 2010a, b).

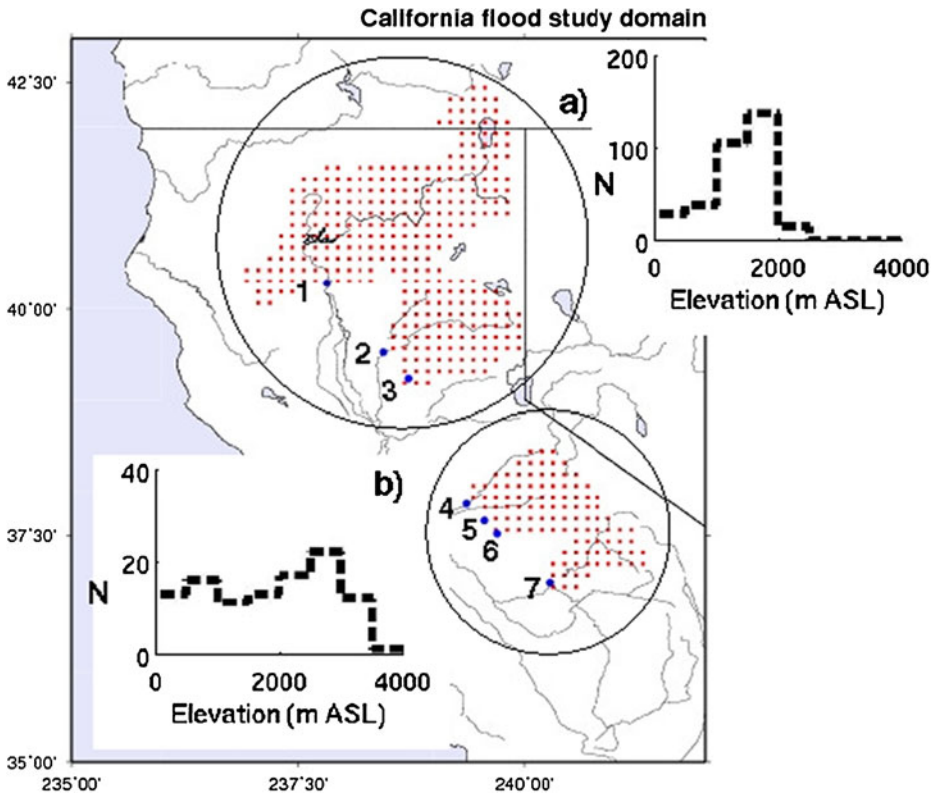


**Fig. 1** California's Northern Sierra Nevada (a) and Southern Sierra Nevada (b). The northern Sierra Nevada consists of the drainage areas from the Sacramento River at Bend Bridge (1), the Feather River at Oroville (2) and the Yuba River at Smartville (3). The southern Sierra Nevada consists of the drainage areas from the four main tributaries of the San Joaquin river: the Stanislaus at New Melones Dam (4), the Tuolumne River at New Don Pedro (5), the Merced at Lake McClure (6) and the San Joaquin at Millerton Lake (7). Histograms show the distribution of the elevations of VIC grid cells

Flood magnitudes of several return periods ( $T$ ), in years, computed from model simulated historical period (1951–1999) were compared with the flood magnitudes at the corresponding return periods based on flows simulated for 2001–2049 and 2051–2099. The 3-day maximum floods for each year were calculated along with their probabilities of exceedance (assigned using the Weibull plotting position) from the three time periods 1951–1999, 2001–2049, and 2051–2099. Then the inverse of the probability (frequency factor,  $K$ ) (Chow et al. 1988; Shabri 2002) was calculated assuming a log-Pearson type III distribution. The  $K$  values were plotted against the base10 logarithm of the 3-day streamflow maximum. A least-squares linear regression was computed from the data along with 99% regression confidence intervals. From these fits and confidence intervals, flood magnitudes with different return periods ranging from 2 years through 50 years were computed from the fitted flood frequency curves from each of the time epochs. A statistical method described in the appendix was used to determine if the change of the flood magnitude under future climate projections with compared to model historical period is significant at a high statistical confidence level (at  $p=0.01$  level).

## 4 Results and discussions

### 4.1 Climate change projections

Water year precipitation and annual temperature values, as deviations from model simulated historical period (1951–1999) normal, from the three GCMs over the NSN and SSN are depicted in Table 1. The changes in annual precipitation and temperature were computed using the area-averaged precipitation and temperature across the drainage areas of NSN and SSN. GCMs used in this study cover a range of climate change sensitivities, so that the projections yield moderate increases of annual temperature between 0.5°C and 1.0°C by 2049, with increases between about 2°C to 3°C by 2099 (Table 1). The GFDL model is warmest, followed by CNRM. Because of naturally occurring decadal and multi-decadal precipitation variations as well as differences among the GCMs, trends in precipitation projections are less steady or unanimous. The GFDL model projects overall drying, whereas the CNRM model projects about a 10% increase in precipitation, by 2049. Precipitation ranges from near historical normal to about 8% reduction by 2099. PCM shows moderate warming and moderate increase of precipitation (Table 1).

The number of winter days with precipitation occurring as snow divided by the total number of winter days with precipitation is calculated as follows. A given wet day (day with precipitation above 0.1 mm), in the period November through March, was classified as a snowy day if snowfall ( $S$ ) was greater than 0.1 mm. As in the VIC (and also in Das et al. 2009),  $S$  was calculated using the equation below:

$$S = \begin{cases} 0 & \text{for } T \geq T_{rain} \\ P \cdot \left( \frac{T - T_{rain}}{T_{snow} - T_{rain}} \right) & \text{for } T_{snow} < T < T_{rain} \\ P & \text{for } T \leq T_{snow} \end{cases}$$

where,  $T$  is the daily average temperature,  $T_{snow}$  is the maximum temperature at which snow falls and  $T_{rain}$  is the minimum temperature at which rain falls. To be consistent with the VIC model simulations, the values of  $T_{snow}$  and  $T_{rain}$  were set to  $-0.5^\circ\text{C}$  and  $0.5^\circ\text{C}$  respectively.

**Table 1** Annual temperature change (°C), annual precipitation change (%), and annual snow days as a percentage of wet days change (%) from historical period (1951–1999) in the Northern Sierra Nevada and Southern Sierra Nevada for the 3 GCMs A2 greenhouse-gas emission scenarios

|                        | $\Delta T$ (°C) |           | $\Delta P$ (%) |           | $\Delta$ Snow days as percentage of wet days (%) |           |
|------------------------|-----------------|-----------|----------------|-----------|--|-----------|
|                        | 2001–2049       | 2051–2099 | 2001–2049      | 2051–2099 | 2001–2049  | 2051–2099 |
| Northern Sierra Nevada |                 |           |                |           |  |           |
| CNRM CM3               | 0.9             | 3.0       | 10.7           | 0.5       | -13.7  | -36.0     |
| GFDL CM2.1             | 1.2             | 3.3       | -0.5           | -10.1     | -16.6  | -47.8     |
| NCAR PCM1              | 0.6             | 2.1       | 3.6            | 3.0       | -10.5  | -39.3     |
| Southern Sierra Nevada |                 |           |                |           |  |           |
| CNRM CM3               | 1.0             | 3.1       | 10.5           | -8.9      | -4.9   | -19.7     |
| GFDL CM2.1             | 1.2             | 3.5       | -2.2           | -14.5     | -7.0   | -25.4     |
| NCAR PCM1              | 0.7             | 2.1       | 4.7            | 5.4       | -4.6   | -16.6     |

The projections yield reductions of winter-total snowy days as a fraction of winter-total days with precipitation (indicating a decrease in days with snowfall); larger changes are projected for NSN and the reductions are amplified by the late 21st century (Table 1).

#### 4.2 Changes in extreme precipitation

There is an indication of increased magnitudes in the 3-day precipitation among the highest values, (longest return intervals), except in NCAR PCM1 (Fig. 2). With respect to the climate projections, in general, there is an increased frequency of the extreme precipitation events for the future projected scenarios, except for the GFDL for SSN which shows extreme precipitation events staying either same or decreasing slightly (Table 2). In terms of the frequency of occurrence of extreme precipitation events, precipitation is considered an extreme event when the daily area-averaged precipitation over the NSN and SSN is larger than 99 percentile values computed from the GCM simulated historical period (1951–

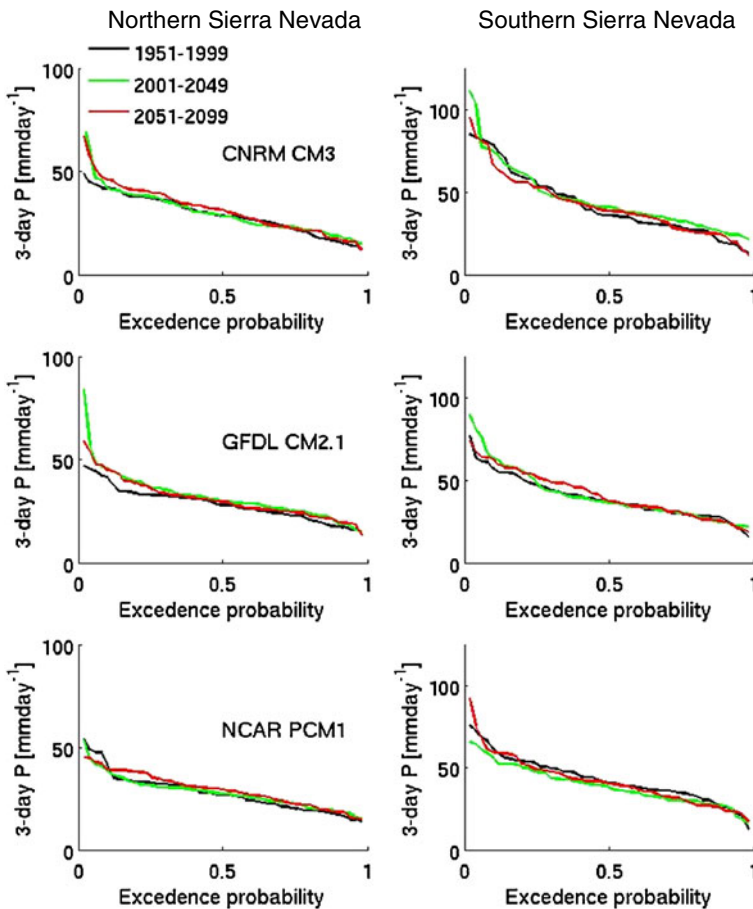


**Fig. 2** Probability distributions for 3-day annual maximum precipitation from CNRM CM3, GFDL CM2.1 and NCAR PCM1 GCMs. Climate change period (2000–2099) from SRES A2 scenarios. 1951–1999 period is from GCM simulated historical period. (Left) Northern Sierra Nevada, (Right) Southern Sierra Nevada

**Table 2** Frequency (number of events per year on average) of extreme precipitation in the Northern Sierra Nevada and Southern Sierra Nevada from three coupled ocean–atmosphere general circulation models, each forced by historical and 21st century greenhouse-gas A2 emission scenarios

|                        | 1951–1999 | 2001–2049 | 2051–2099 |
|------------------------|-----------|-----------|-----------|
| Northern Sierra Nevada |           |           |           |
| CNRM CM3               | 2.7       | 3.8       | 4.2       |
| GFDL CM2.1             | 2.7       | 3.0       | 3.2       |
| NCAR PCM1              | 2.7       | 3.5       | 3.5       |
| Southern Sierra Nevada |           |           |           |
| CNRM CM3               | 2.7       | 4.0       | 3.2       |
| GFDL CM2.1             | 2.7       | 2.6       | 2.7       |
| NCAR PCM1              | 2.7       | 3.0       | 3.3       |

1999). The climate model simulations yield increases in extreme precipitation events by about 11% to 40% by 2049 for NSN, and between 18% through 55% by 2099. For SSN, the changes of extreme precipitation frequency are about –4% through 48% by 2049, and 0% through 22% by 2099 (Table 2). Furthermore, when aggregating the extreme precipitation events for the winter period (DJF), climate models suggest an increase in the frequency of extreme precipitation events for the projected period (2000–2099) in both the NSN and SSN. Thus, overall, the projections tend towards larger storm totals and more frequent extreme-precipitation events.

#### 4.3 Flood magnitudes

We begin our evaluations by comparing probability distributions for 3-day annual streamflow from VIC simulations as driven by downscaled climate model meteorology from CNRM CM3, GFDL CM2.1 and NCAR PCM1 GCMs for NSN and SSN. Annual 3-day maximum flows increase for the longest return periods (largest floods), except for NCAR PCM1 for the period 2051–2099 which shows a slight decrease (Fig. 3).

A flood frequency analysis of the 3-day floods as simulated by VIC in response to the historical observed meteorology is shown in Fig. 4 (*top panels*). The climate change impact on the flood discharge magnitude was evaluated by comparing flood frequency curves estimated from the future simulations (Fig. 4) to those estimated from historical simulations. Table 3 presents flood discharges for various return periods, ranging from 2-years to 50-years, in absolute and relative terms. The hypothesis that the best prediction of flood discharge for a certain return period  $T$  in years ( $Q_T$ ) from the historical period (1951–1999) was statistically different from the best prediction of  $Q_T$  under the future climate was tested using a statistical method described in the [appendix](#). As can be seen, for the NSN there is a general increase in the  $Q_T$  in the future climate. These increases are statistically significant (at  $p=0.01$  level) for the CNRM, GFDL simulations of the first half of the 21st century (2001–2049) while the increases of  $Q_T$  for all return periods are statistically significant for the late period of the 21st century (2051–2099) (Table 3). For SSN, the increase of flood discharges for all the return periods for CNRM, and flood discharges with more frequent return periods (up to 5-years) for GFDL are statistically significant for the first half of 21st century (2001–2049). PCM1 simulated flood discharges for the 2001–2049 epoch declined compared to model historical. However, by 2051–2099, there is an increase in the 3-day flows for the all 3-GCMs, including the GCM models that project 8–15% declines in overall precipitation, and the increases are statistically significant with high confidence.

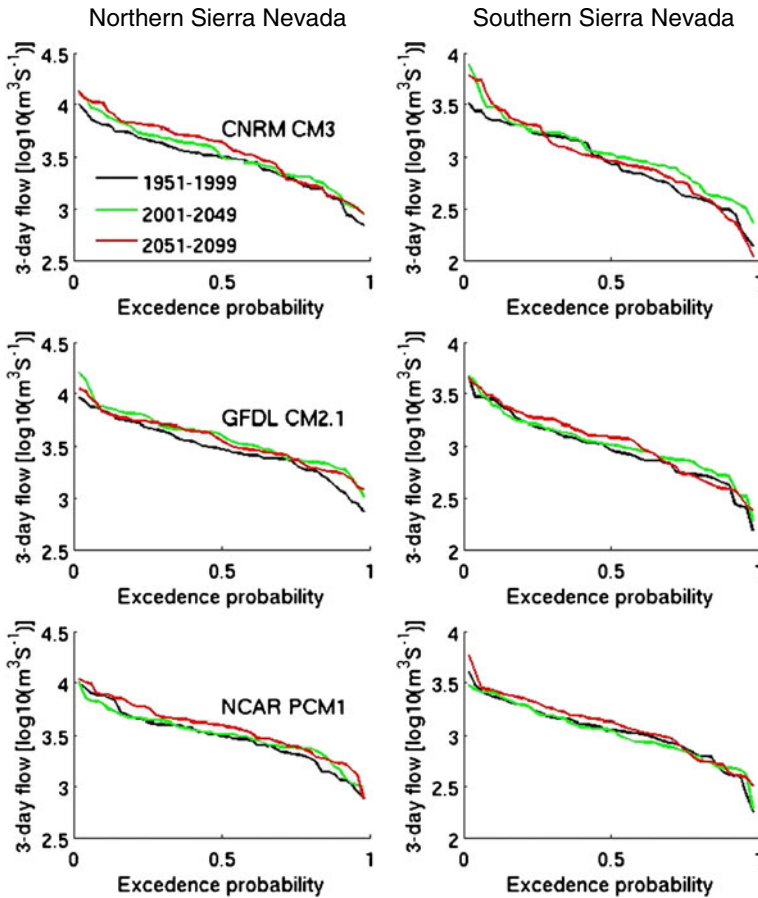


**Fig. 3** Same as Fig. 2, except using 3-days maximum annual streamflows as simulated by downscaled meteorology from CNRM CM3, GFDL CM2.1 and NCAR PCM1 GCMs

#### 4.4 Flood occurrences

Historically, most of the floods in California's NSN have occurred from November to March (Fig. 5, *left top panel*). As in the observations, the largest simulated floods occurred during winter (DJF) and they correspond to so-called "pineapple express" events—in which strong low-level Pacific jets transport copious water vapor and warm temperatures to the West Coast (Cayan and Peterson 1989; 1993; Pandey et al. 1999; Cayan and Riddle 1992; Dettinger 2004; Mo et al. 2005; Ralph et al. 2006; Dettinger 2011). During spring (MAM), smaller floods are common and usually are driven by snowmelt on sunny days. These two kinds of floods in the SSN were evaluated in terms of whether it rained or not during the days of the flood (Fig. 5, *right top panel*). There are "wet" or precipitation-dominated floods, mostly in winter, and "dry" or snowmelt-dominated floods, mostly in summer (see also Roos 2006). As in the NSN, the largest floods in the SSN occur during the winter (DJF) corresponding to precipitation-dominated floods, associated with midlatitude, winter storms. Snowmelt-dominated floods occur mainly during the spring-summer (MJJ) and are associated with high-

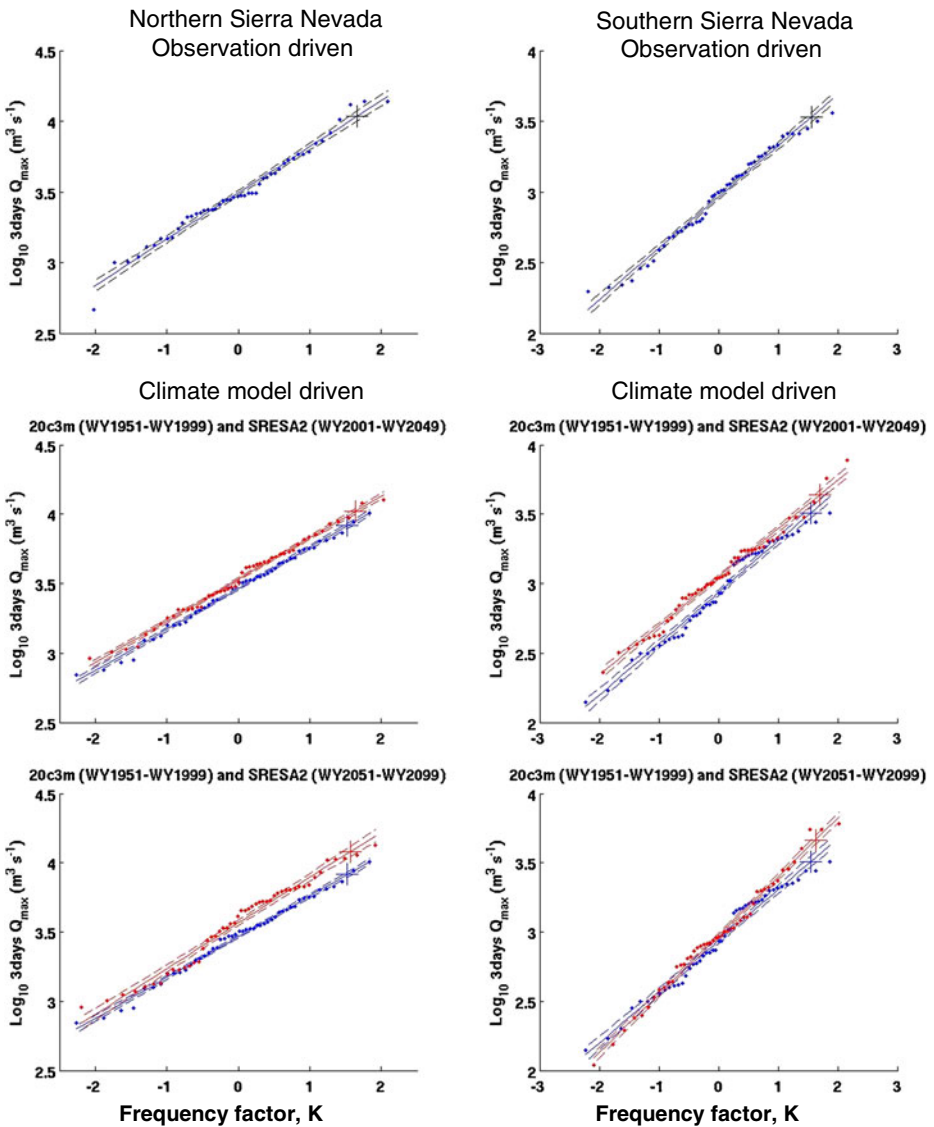


**Fig. 4** Frequency of the three-day annual maximum streamflows. Log Pearson III distributions have been fitted to each flood series. Dotted curves: confidence limit for regression line (at 0.01 confidence level). Panels on first row shows flood frequency curves developed using observed meteorology driven VIC simulated streamflows from the period 1951–1999. Second and third row panels compares flood Frequency curves developed using downscaled CNRM CM3 driven VIC simulated streamflows from period 1951–1999 (blue curves) with time periods 2001–2049 and 2051–2099. In the figures, “+” symbol mark flood magnitude with 20-years return period. (*Left*) Northern Sierra Nevada, (*Right*) Southern Sierra Nevada

pressure patterns over the western US that bring higher than normal temperatures and cloud-free days through atmospheric subsidence.

Figure 5 (second to fourth row panels) illustrates floods in Californian NSN and SSN using VIC simulated streamflows as driven by the downscaled CNRM meteorology for the periods 1951–1999, 2001–2049 and 2051–2099. A few of the projected floods have

**Table 3** Three-day maximum floods from flood frequency analyses using log-Pearson III distributions; boldface where statistically different from floods in 1951–1999 period (at  $p=0.01$ ). Numbers in italics indicate flood discharges are decreased compared to 1951–1999 period

| T (In Years)           | 3-days flood discharge |                     |                     | Percentage difference      |                           |
|------------------------|------------------------|---------------------|---------------------|----------------------------|---------------------------|
|                        | Q20c3m                 | Qearly              | Qlate               | (Qearly-Q20c3m)/<br>Q20c3m | (Qlate-Q20c3m)/<br>Q20c3m |
|                        | (WY1951–<br>WY1999)    | (WY2001–<br>WY2049) | (WY2051–<br>WY2099) | (%)                        | (%)                       |
| Northern Sierra Nevada |                        |                     |                     |                            |                           |
| CNRM CM3               |                        |                     |                     |                            |                           |
| 2                      | 3050                   | <b>3410</b>         | <b>3800</b>         | 12                         | 25                        |
| 5                      | 5220                   | <b>6060</b>         | <b>7020</b>         | 16                         | 34                        |
| 10                     | 6750                   | <b>8170</b>         | <b>9500</b>         | 21                         | 41                        |
| 20                     | 8240                   | <b>10440</b>        | <b>12080</b>        | 27                         | 47                        |
| 50                     | 10190                  | <b>13730</b>        | <b>15680</b>        | 35                         | 54                        |
| GFDL CM2.1             |                        |                     |                     |                            |                           |
| 2                      | 3110                   | <b>3800</b>         | <b>3590</b>         | 22                         | 15                        |
| 5                      | 5220                   | <b>6430</b>         | <b>5830</b>         | 23                         | 12                        |
| 10                     | 6730                   | <b>8550</b>         | <b>7510</b>         | 27                         | 12                        |
| 20                     | 8230                   | <b>10880</b>        | <b>9260</b>         | 32                         | 13                        |
| 50                     | 10220                  | <b>14350</b>        | <b>11730</b>        | 40                         | 15                        |
| NCAR PCM1              |                        |                     |                     |                            |                           |
| 2                      | 3070                   | <b>3250</b>         | <b>3750</b>         | 6                          | 22                        |
| 5                      | 5200                   | <i>4980</i>         | <b>6150</b>         | −4                         | 18                        |
| 10                     | 6770                   | <i>6120</i>         | <b>7850</b>         | −10                        | 16                        |
| 20                     | 8380                   | <i>7190</i>         | <b>9520</b>         | −14                        | 14                        |
| 50                     | 10590                  | <i>8550</i>         | <b>11740</b>        | −19                        | 11                        |
| Southern Sierra Nevada |                        |                     |                     |                            |                           |
| CNRM CM3               |                        |                     |                     |                            |                           |
| 2                      | 910                    | <b>1080</b>         | <b>960</b>          | 19                         | 5                         |
| 5                      | 1790                   | <b>2170</b>         | <b>2150</b>         | 21                         | 20                        |
| 10                     | 2480                   | <b>3160</b>         | <b>3280</b>         | 27                         | 32                        |
| 20                     | 3220                   | <b>4360</b>         | <b>4620</b>         | 35                         | 43                        |
| 50                     | 4260                   | <b>6320</b>         | <b>6780</b>         | 48                         | 59                        |
| GFDL CM2.1             |                        |                     |                     |                            |                           |
| 2                      | 970                    | <b>1070</b>         | <b>1120</b>         | 10                         | 15                        |
| 5                      | 1820                   | 1880                | <b>2130</b>         | 3                          | 17                        |
| 10                     | 2500                   | 2510                | <b>2940</b>         | 0                          | 18                        |
| 20                     | 3230                   | <i>3190</i>         | <b>3810</b>         | −1                         | 18                        |
| 50                     | 4290                   | <i>4170</i>         | <b>5070</b>         | −3                         | 18                        |
| NCAR PCM1              |                        |                     |                     |                            |                           |
| 2                      | 1140                   | <i>1080</i>         | <b>1230</b>         | −5                         | 8                         |
| 5                      | 1910                   | <i>1800</i>         | <b>2190</b>         | −6                         | 15                        |
| 10                     | 2430                   | <i>2320</i>         | <b>2930</b>         | −5                         | 21                        |
| 20                     | 2910                   | <i>2830</i>         | <b>3720</b>         | −3                         | 28                        |
| 50                     | 3510                   | 3510                | <b>4860</b>         | 0                          | 38                        |

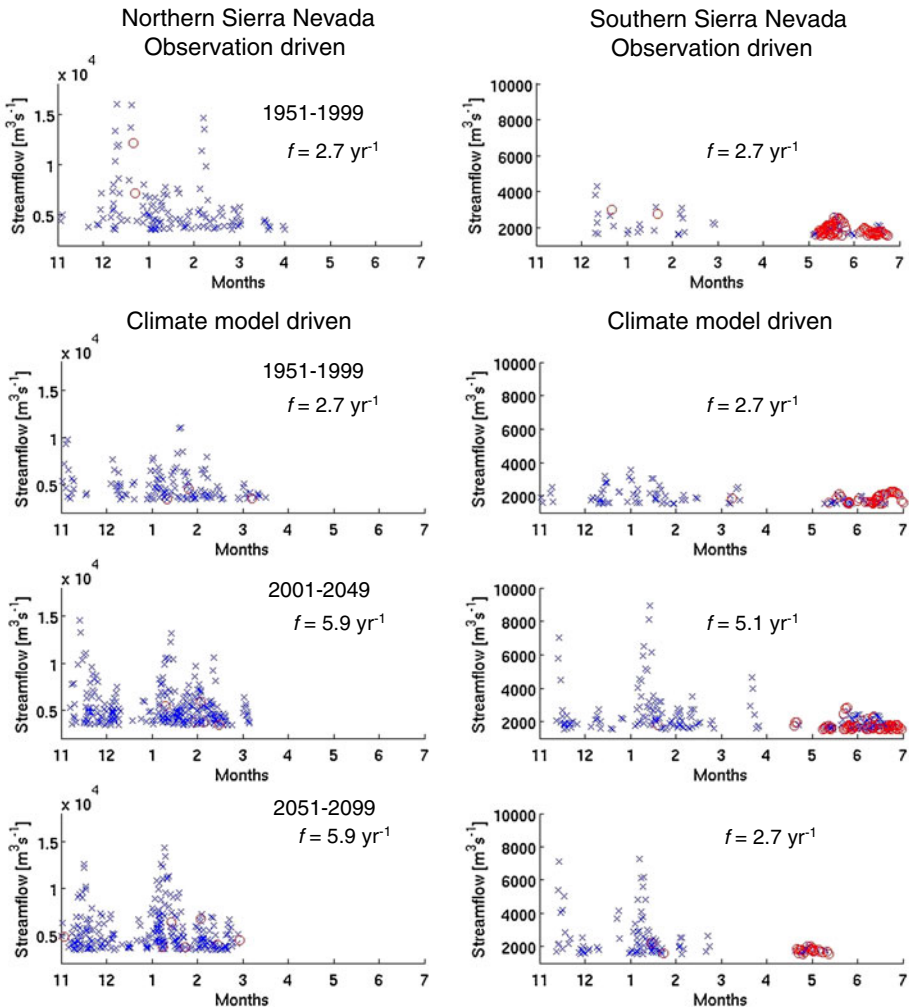


**Fig. 5** Floods in Californian Northern Sierra Nevada (*Left*) and Southern Sierra Nevada (*Right*). Panels on first row shows floods using observed meteorology driven VIC simulated streamflows from the period 1951–1999. Second and third row panels show floods using downscaled CNRM CM3 driven VIC simulated streamflows from periods 1951–1999, 2001–2049 and 2051–2099. Numbers (*f*) in each panel indicate frequency of the floods per year on average. In the figure, “X” symbols are precipitation-driven floods and red circles are snowmelt driven floods. Flood is defined if streamflow in a given day for the period November through July is larger than 99 percentile value computed from the time period 1951–1999

unprecedentedly large magnitudes compared to the historical simulations. Table 4 presents the frequency (number of events per year on average) of flood events in the NSN and SSN. In general, the frequency of floods increases in the future, except under the GFDL climate in SSN where numbers of flood events remain constant or decline slightly; recall that GFDL is the GCM (among those considered here) that dries most in the 21st century. There is no clear indication of a change in the seasonality of the floods; however the simulations suggest declining numbers of snow-melt driven floods for SSN under projected climate, particularly in the late 21st century (2051–2099).

**Table 4** Frequency (number of events per year on average) of the floods in the Northern Sierra Nevada and Southern Sierra Nevada from three coupled ocean–atmosphere general circulation models, each forced by historical and 21st century greenhouse-gas A2 emission scenarios

|                        | 1951–1999 | 2001–2049 | 2051–2099 |
|------------------------|-----------|-----------|-----------|
| Northern Sierra Nevada |           |           |           |
| CNRM CM3               | 2.7       | 5.9       | 5.9       |
| GFDL CM2.1             | 2.7       | 2.6       | 3.0       |
| NCAR PCM1              | 2.7       | 3.6       | 6.4       |
| Southern Sierra Nevada |           |           |           |
| CNRM CM3               | 2.7       | 5.1       | 2.7       |
| GFDL CM2.1             | 2.7       | 2.5       | 2.4       |
| NCAR PCM1              | 2.7       | 2.8       | 4.0       |

#### 4.5 Mechanisms of change in flood risk

Although changes in flood magnitude and occurrence ultimately result from changes in storm sizes (Dettinger 2011), temperatures, and frequencies, there are other factors, including rainfall-receiving area, areas where rain falls on snow, and antecedent soil moisture conditions that also influence flood characteristics and changes under climate change. In this section, several possible mechanisms for each flood characteristic change are discussed.

Relationships between precipitation and areas receiving rainfall are illustrated by plotting the conditions during all storm events historically and in first and second halves of the 21st Century for NSN (Fig. 6) and SSN (Fig. 7). To make these plots, for each flood event, precipitation is summed over 3 consecutive days and the fraction of catchment receiving rain (rather than snow) is averaged, where the 3-day windows constitute the identified flood day, the day before, and the day before that. Notably, comparison of panels along the rows in Figs. 6 and 7 shows that some projected storms have precipitation totals with unprecedentedly large magnitudes compared to the historical simulations. However, more generally, the slopes of the clouds of dot in Figs. 6 and 7 indicate that larger floods (represented by larger circle sizes in the figures) have typically been associated with storms with large precipitation totals. Nonetheless, there is considerable scatter and some large floods have occurred during smaller storms. Also a few storms with larger precipitation totals produce small floods. This kind of scatter appears across the almost the full range of rain-receiving areas from little rainy area to entirely rainy. Consequently we infer that differences in the saturation of soils and land surfaces when the various storms arrived also probably play important roles in determining whether many storms are flood-generating versus non-flood-generating. In particular, in the moderately warmer climates projected for the 21st Century, whether or not the climate is drier or wetter overall, snowpacks typically continue to be formed each winter, although they may be less persistent and thinner. The snowpacks presumably are wetter and experience more frequent midwinter melt cycles, so that soils in the wintertime Sierra Nevada may be wetter than historical as a result of more frequent percolation of winter snowmelts into the soils (Dettinger et al. 2009).

To further explore the role of areas that receive rainfall in the flood-generating storms, we computed basin area receiving rainfall as a percentage of total basin area for each rainfed flood (X's in Fig. 5) for NSN and SSN. Table 5 lists the average areas that receive

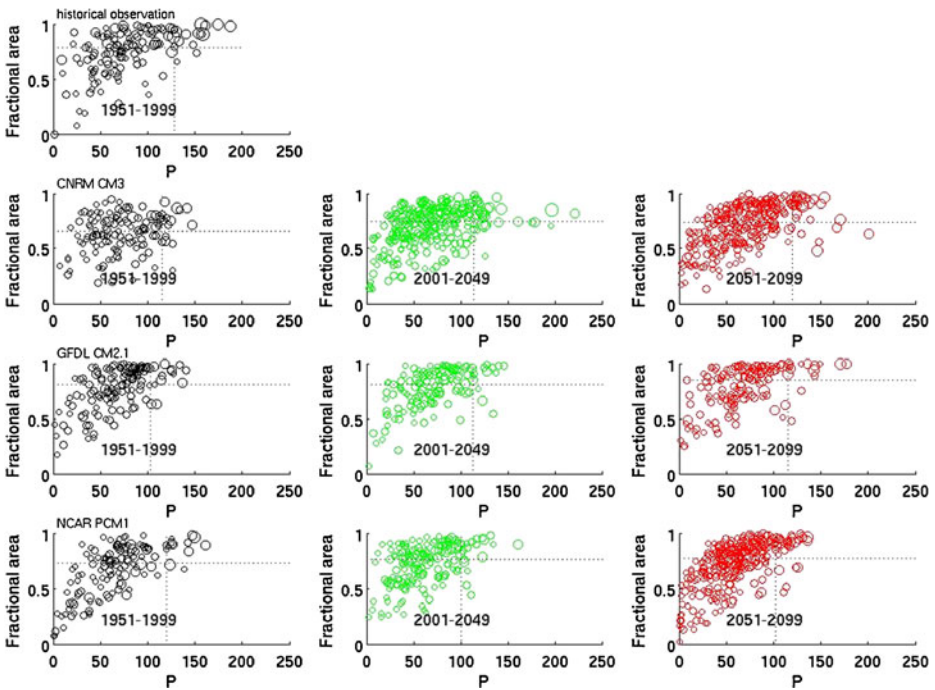


**Fig. 6** Precipitation and fractional area that receives rainfall are plotted for each of the flood events, for Northern Sierra Nevada. Panel in first row shows result from observational driven VIC simulation. Second, third and fourth row panels show results using three climate models. For each of the flood events, precipitation (fractional area) is summed (averaged) for 3-consecutive days: the identified flood day, the day before, and the day before that. In the figure, symbol size varies depending on the flood day streamflow. Dotted vertical lines show 90 percentile values of precipitation from each flood population time period. Dotted horizontal lines show 50 percentile values of fractional area from each flood population time period

rainfall, averaged over the rainfed floods in the model historical period (1951–1999) and from climate projections epochs (2001–2099). The extent to which a given amount of warming increases the rainfall receiving areas differs from basin to basin depending on the topography of the basins. Altitudes in SSN rise much higher than in NSN. As a result, the NSN is more dominated by catchment areas at middle to low altitudes, and thus receives rain on larger fractions of the basin in many storms, than in SSN. As in Table 5, except for one exception, there are increases in areas that receive rainfall during the flood days under climate change projections in all three GCMs in both NSN and SSN, by 3% to 15% for NSN and 7% to 30% for SSN by 2051–2099.

McCabe et al. (2007) have shown that, historically, with warming in the western US, the occurrence of rain-on-snow events has declined at low sites and increased at high sites. The decreasing numbers of low-altitude rain-on-snow events reflect declining periods when snow is on the ground available to receive rain. The average percentages of basin area receiving rainfall when there is an antecedent snowpack on the ground, computed from the VIC simulations, for the precipitation driven flood days, as shown in Fig. 5, indicate considerable decreases of the rain-on-snow areas for NSN, especially for the late 21st century. Surprisingly, there is not much change for SSN, perhaps due to countervailing influences of low areas with less snow to be rained upon and high areas with snow that are reached more frequently by rain under the projected warming trends. These countervailing

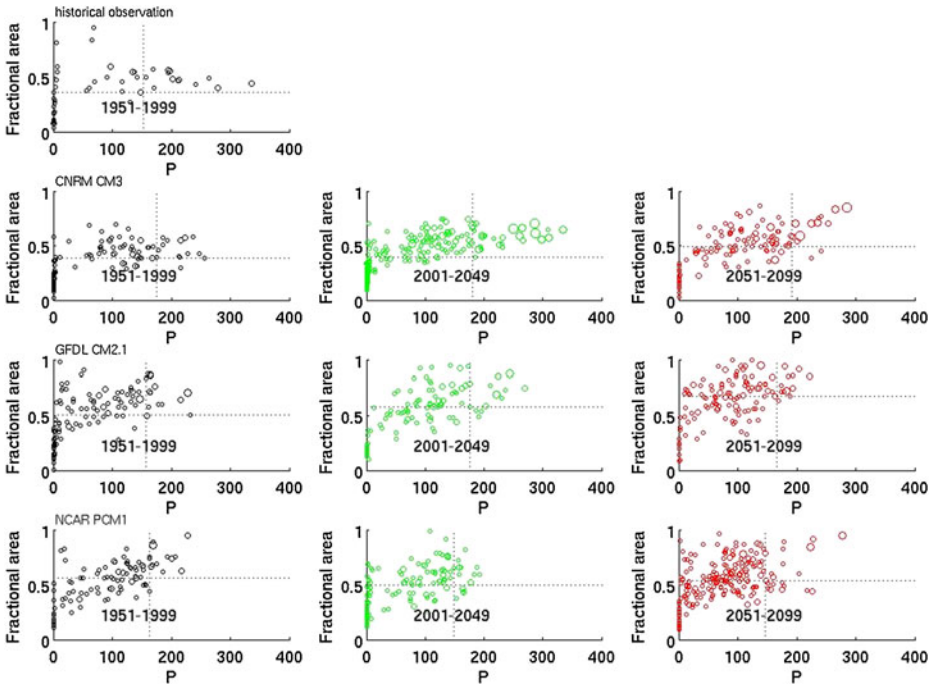


Fig. 7 Same as Fig. 6, except for the Southern Sierra Nevada

influences may be more important in the SSN than in the NSN because of the larger range of elevations in the SSN.

As long as there is generally some snow on the ground in the catchment, warming is likely to increase the number of occasions when the snow will melt even in mid-winter. To investigate the role of antecedent soil moisture in the generated floods, we compared cumulative distribution functions of antecedent soil moisture 2 days prior to the flood events simulated by VIC. These antecedent soil moisture contents increased in the NSN only under the CNRM projections (soil moisture stayed the same or decreased in the other two GCMs). In the SSN, antecedent soil moisture increased in two of the three GCMs (*not shown*).

### 5 Summary and conclusions

This study investigated how future climate changes might affect flood risk in the Sierra Nevada Mountains of California. The study uses downscaled daily precipitation and temperature simulations from three global climate models (GCMs) under an accelerating (A2) greenhouse-gas emissions scenario, to drive the VIC hydrologic model for catchments on the west slopes of the Sierra Nevada Mountains. In making VIC runs from historical and from projected climate change GCM simulations, we explore possible changes in annual maximum 3-day flood magnitudes and frequencies of floods greater than selected historical thresholds.

Analyses of future projections of flooding reveal a general tendency toward increases in the magnitudes of 3-day flood events. By the end of the 21st Century, all three projections yield larger floods for both the moderate elevation Northern Sierra Nevada (NSN) watershed and for the high elevation Southern Sierra Nevada (SSN) watershed, even for

**Table 5** River basin area that receives rainfall (area with average temperature larger than 0.5°C), as a percentage of total River basin area. Table also contains percentage of basin area that receives Rainfall on Snow. The values are averaged from all precipitation-driven floods, in the Northern Sierra Nevada and Southern Sierra Nevada, under model historical simulation and climate change projections from three coupled ocean–atmosphere general circulation models. In parentheses, changes are computed from model simulated historical period (1951–1999)

|   | 1951–1999 | 2001–2049    | 2051–2099    |
|---|-----------|--------------|--------------|
| Percentage of basin area that receives Rainfall         |           |              |              |
| Northern Sierra Nevada                                  |           |              |              |
| CNRM CM3  | 55.2      | 64.0 (+15.9) | 60.8 (+10.1) |
| GFDL CM2.1  | 66.0      | 66.2 (+0.3)  | 68.3 (+3.5)  |
| NCAR PCM1   | 54.8      | 59.7 (+8.9)  | 64.0 (+16.8) |
| Southern Sierra Nevada                                  |           |              |              |
| CNRM CM3  | 34.6      | 38.7 (+11.8) | 45.1 (+30.3) |
| GFDL CM2.1  | 44.7      | 51.0 (+14.1) | 55.3 (+23.7) |
| NCAR PCM1   | 45.6      | 43.4 (−4.8)  | 48.9 (+7.2)  |
| Percentage of basin area that receives Rainfall on Snow |           |              |              |
| Northern Sierra Nevada                                  |           |              |              |
| CNRM CM3  | 23.9      | 24.9 (+4.2)  | 12.7 (−46.9) |
| GFDL CM2.1  | 15.9      | 11.3 (−28.9) | 8.9 (−44.0)  |
| NCAR PCM1   | 17.2      | 12.5 (−27.3) | 10.2 (−40.7) |
| Southern Sierra Nevada                                  |           |              |              |
| CNRM CM3  | 12.3      | 15.7 (+27.6) | 11.6 (−5.7)  |
| GFDL CM2.1  | 16.9      | 11.5 (−32.0) | 15.4 (−8.9)  |
| NCAR PCM1   | 13.7      | 15.6 (+13.9) | 14.4 (+5.1)  |

GCM simulations with 8–15% declines in overall precipitation. The increases in flood magnitude are statistically significant (at  $p=0.01$  level) for all three GCMs for the period 2051–2099 (Fig. 4 and Table 3). By the end of the 21st Century, the magnitudes of the largest floods increase to 110% to 150% of historical magnitudes. Realistically, the half-century windows used to estimate changing 50-year flood magnitudes are short. However, we wanted to present here indications of the potential for changes in magnitudes of the largest floods under medium-high greenhouse-gas emissions with attendant medium-high climate changes over California. As part of the analysis described here, we also computed changes in flood magnitudes with return periods 2-years, 5-years, 10 years, and 20-years (as shown in Table 3), return periods more confidently estimated with the half-century windows analyzed. These more confidently estimated results (for smaller flood levels) corroborate the 50-year flood changes presented in the body of this paper.

Large winter (DJF) floods have occurred during the historical period in both the NSN and SSN (Fig. 5, *top panels*). These winter floods are most often outcomes from Pacific storm-generated immediate runoff from the warmer, rainfall affected parts of the Sierra watersheds. Spring floods in the NSN often arise from storms and conditions similar to the DJF floods, but with lower magnitudes. In contrast, in the SSN, spring (MJJ) floods do not often occur during storm events and instead are more commonly snowmelt fed. These MJJ floods rise to magnitudes comparable to the DJF floods. In the projections, the frequency of floods (above historical 99th percentile thresholds) increases under the CNRM and PCM1 climate changes, while under the GFDL climate, which has the strongest drying trend over

the 21st Century, the frequency remained constant or declined slightly. The VIC simulations have a tendency to yield fewer snowmelt driven floods for SSN, particularly under the late 21st century (2051–2099). In general there is a projected tendency for more frequent winter rainfall generated floods and fewer snowmelt floods as climate warms.

The increased flood frequencies appear to derive from three factors: increases in the sizes of the largest storms, increased storm frequencies, and days with more precipitation falling as rain and less as snow (Figs. 6 and 7; Table 5). Increases in antecedent winter soil moisture also play a role in some areas, particularly in the SSN. Thus, several mechanisms may end up contributing simultaneously to increased flood hazards in California's western Sierra Nevada catchments. The particular mixes of influences on flood magnitudes and frequencies at the multi basin scales considered here are unlikely to apply everywhere at smaller scales, from basin to basin, and do not even appear to be consistent from climate-change scenario to scenario. Thus more detailed simulations and analyses, with broader ensembles of climate-change projections, will be needed to develop much confidence in real-world, actionable predictions about flood-regime changes.

The varied results here emphasize the uncertainties related to the present generation of GCM's, manifested in different magnitudes of warming and quite strongly different changes (neutral to negative) in precipitation over the 21st Century. However, the current results present us with three separate versions of the future of floods (one from each of the GCMs). The differences between flood responses to the various scenarios considered here are not unexpected, as flood is a result of combination from precipitation, temperature and antecedent catchment conditions. Future research involving GCMs (Dettinger 2005; Maurer 2007; Pierce et al. 2009), downscaling (Maurer et al. 2010a) and hydrological model simulations (Maurer et al. 2010b) will be needed to objectively merge results from several GCMs into a single master estimate of changing flood frequencies and their associated uncertainties. (see e.g. Raff et al. 2009). Nonetheless, the size of changes simulated here, under the different projections, are evidence that plausible levels of 21st Century climate change are likely to affect future flood magnitudes and frequencies in significant ways. The strong tendencies for the several scenarios investigated here to agree in certain qualitative and even quantitative ways also suggests that some strong consensus regarding future flood probabilities may be possible outcomes from such expansions of the research agenda illustrated here.

VIC is a macroscale hydrologic model and its use in the present study is only to assess, through a rather coarse lens, flood tendencies that might occur under climate changes. We would not suggest that the quantitative flood discharges computed using VIC be used for structural designs or details of flood management. From these analyses, we conclude (as others have, for example Dettinger et al. 2004; Miller et al. 2003; Anderson et al. 2006; Dettinger et al. 2009; Raff et al. 2009) that flood regimes in Californian Sierra Nevada are vulnerable to change with future climate change. With the models used here, flood magnitudes and frequencies tend overall (but not universally) to increase, even under scenarios with significant drying. A common feature among the projections is warming; however, tendencies towards intensification of the most severe storms also are common (Dettinger 2011). These broad qualitative mechanisms and flood responses may prove to be robust, but precision in the changing flood frequency estimates is not yet available. Flood frequency estimation procedures that more directly incorporate non-stationarity will need to be developed to permit observations-based frequency estimation for detailed planning of flood management under future climate change (see also Griffis and Stedinger 2007; Sivapalan and Samuel 2009; Raff et al. 2009). Precision simulation-based flood frequency estimation will have to await more precise climate-change projections and hydrologic models of flood responses.

**Acknowledgments** We thank the Program for Climate Model Diagnosis and Intercomparison (PCMDI) and the WCRP’s Working Group on Coupled Modelling (WGCM) for the WCRP CMIP3 multi-model dataset. Support of this dataset is provided by the Office of Science, U.S. Department of Energy. We acknowledge particularly the GCM modeling groups at CNRM, NCAR and GFDL for GCM output. Thanks to Michael Anderson and John T. Andrew at California Department of Water Resources for their valuable discussions. We thank three anonymous reviewers and editors for useful comments. The study was supported by both the CALFED Bay-Delta Program-funded postdoctoral fellowship grant provided to TD and the California Energy Commission-funded California Climate Change Center. Partial salary support for TD from Environment and Sustainability Initiative at UC San Diego (now Sustainability Solutions Institute) through a seed funding grant is also acknowledged. The California Energy Commission PIER Program through the California Climate Change Center, the NOAA RISA Program via the CNAP RISA, and DOE through grant DE-SC0002000, provided partial salary support for DC. Much of the contribution of HH was done while he was a Project Scientist at SIO. He is now partially funded through research projects VI-805-A9-224 and VI-808-A9-180 of the University of Costa Rica.

**Appendix: Test of significance for flood magnitude**

For two regression-based estimates of log-transformed flood magnitudes with recurrence interval of  $r$  years,  $f_1 \sim N(m_1, s_1)$  (e.g., from simulated historical annual-flood series) and  $f_2 \sim N(m_2, s_2)$  (from simulated future annual-flood series), the probability that  $f_2 > f_1$  is

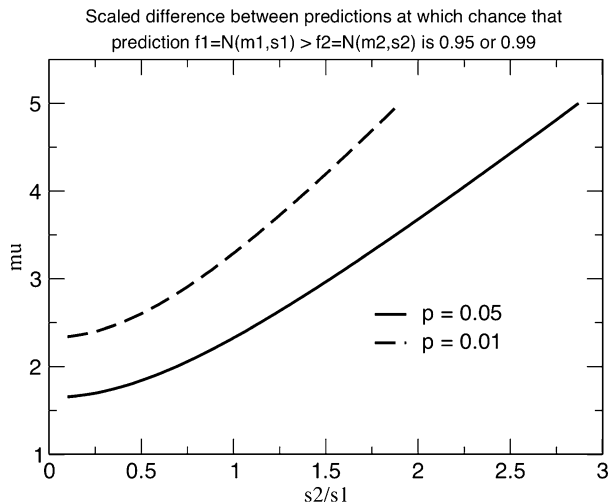
$$\int_{-\infty}^{+\infty} \frac{1}{\sqrt{2\pi}s_2} e^{-\frac{1}{2}\left(\frac{x-m_2}{s_2}\right)^2} \int_{-\infty}^x \frac{1}{\sqrt{2\pi}s_1} e^{-\frac{1}{2}\left(\frac{y-m_1}{s_1}\right)^2} dy dx$$

or, after rearranging the problem in a more readily generalized form,

$$\int_{-\infty}^{+\infty} \frac{s_1}{\sqrt{2\pi}s_2} e^{-\frac{1}{2}(x-(m_2-m_1)/s_1)^2 s_1^2/s_2^2} \left[ \frac{1}{\sqrt{2\pi}} \int_{-\infty}^x e^{-\frac{y^2}{2}} dy \right] dx$$

Upon numerical integration of this distribution for various values of  $(s_2/s_1)$  and  $(m_2-m_1)/s_1$ , and then identification of the values  $\mu_{s_2/s_1}$  of  $(m_2-m_1)/s_1$  corresponding to  $\text{Prob}(f_2 > f_1) = 0.95$  or  $0.99$  as a function of  $s_2/s_1$  (Fig. 8), the null hypothesis that  $f_2 \leq f_1$  can be rejected (at  $p = 0.05$  and  $p = 0.01$  levels) when  $(m_2-m_1)/s_1 > \mu_{s_2/s_1}$ .

**Fig. 8** Values  $\mu=(m_2-m_1)/s_1$  as a function of  $s_2/s_1$  where the probability that  $f_1 \sim N(m_1, s_1)$  is greater than  $f_2 \sim N(m_2, s_2)$  is 0.95 or 0.99



## References

- Anderson M, Miller NL, Heiland B, King J, Lek B, Nemeth S, Pranger T, Roos M (2006) Climate change impacts on flood management. Chapter 6, Progress on incorporating climate change into management of California's water resources. California Department of Water Resources Progress Report. Governor's Climate Initiative Report
- Barnett TP, Pierce DW, Hidalgo HG, Bonfils C, Santer BD, Das T, Bala G, Wood A, Nazawa T, Mirin A, Cayan D, Dettinger M (2008) Human-induced changes in the hydrology of the western US. *Science*. doi:10.1126/science.1152538
- Bonfils C, Duffy PB, Santer BD, Wigley TML, Lobell DB, Phillips TJ, Doutriaux C (2008) Identification of external influences on temperatures in California. *Clim Chang* 87(Suppl 1):S43–S55. doi:10.1007/s10584-007-9374-9
- Brekke LD, Maurer EP, Anderson JD, Dettinger MD, Townsley ES, Harrison A, Pruitt T (2009) Assessing reservoir operations risk under climate change. *Water Resour Res* 45:W04411. doi:10.1029/2008WR006941
- Cayan DR, Peterson DH (1989) The influence of North Pacific atmospheric circulation on streamflow in the West. *PACLIM*. AGU monograph, No 55, American Geophysical Union. 375–397
- Cayan DR, Peterson DH (1993) Spring climate and salinity in the San Francisco Bay Estuary. *Water Resour Res* 2:293–303
- Cayan DR, Riddle L (1992) Atmospheric circulation and precipitation in the Sierra Nevada: Proceedings, International Symposium on Managing Water Resources During Global Change. American Water Resources Association, Reno, Nevada, Nov 1–5
- Cayan DR, Dettinger MD, Hanson R, Brown T, Westerling A (2001) Investigation of climate change impacts on water resources in the California region, Department of Energy Accelerated Climate Prediction Initiative (ACPI) Progress Report, 1/19/01, Scripps Institution of Oceanography, U.S. Geological Survey, Desert Research Institute, p 26
- Cayan DR, Maurer EP, Dettinger MD, Tyree M, Hayhoe K (2008a) Climate change scenarios for the California region. *Clim Chang* 87(suppl 1):21–42. doi:10.1007/s10584-007-9377-6
- Cayan DR, Lures AL, Franco G, Hanemann M, Croes B, Vine E (2008b) Overview of the California climate change scenarios project. *Clim Chang* 87(suppl 1):S1–S6. doi:10.1007/s10584-007-9352-2
- Cayan D, Tyree M, Dettinger M, Hidalgo H, Das T, Maurer E, Bromirski P, Graham N, Flick R (2009) Climate change scenarios and sea level rise estimates for the California 2009 climate change scenarios assessment. California Climate Change Center. CEC-500-2009-014-F, p 64. Available online: <http://www.energy.ca.gov/2009publications/CEC-500-2009-014/CEC-500-2009-014-F.PDF>
- Cayan DR, Das T, Pierce DW, Barnett TP, Tyree M, Gershunov A (2010) Future dryness in the southwest US and the hydrology of the early 21st century drought. *Proc Natl Acad Sci* 107(50):21271–21276. doi:10.1073/pnas.0912391107
- Cherkauer KA, Bowling LC, Lettenmaier DP (2003) Variable infiltration capacity cold land process model updates. *Global Plan. Change* 38:151–159
- Chow VT, Maidment DR, Mays LW (1988) Applied hydrology. McGraw-Hill International Editions, Civil Engineering Series
- Chung F, Anderson J, Arora S, Ejeta M, Galef J, Kadir T, Kao K, Olson A, Quan C, Reyes E, Roos M, Seneviratne S, Wang J, Yin H, Blomquist N (2009) Using future climate projections to support water resources decision making in California, California Energy Commission Technical Report CEC-500-2009-052-F, August 2009
- Daly C, Neilson RP, Phillips DL (1994) A statistical-topographic model for mapping climatological precipitation over mountainous terrain. *J Appl Meteorol* 33:140–158
- Das T, Hugo G, Hidalgo MD, Dettinger DR, Cayan DW, Pierce CB, Barnett TP, Bala G, Mirin A (2009) Structure and Detectability of trends in hydrological measures over the Western US. *J Hydrometeorol* 10:871–892. doi:10.1175/2009JHM1095.1
- Dettinger MD (2004) Fifty-two years of “pineapple-express” storms across the West Coast of North America. US Geological Survey, Scripps Institution of Oceanography for the California Energy Commission. PIER project report. CEC-500-2005-004, 20 Pp. Available online at <http://www.energy.ca.gov/2005publications/CEC-500-2005-004/CEC-500-2005-004.PDF>
- Dettinger MD (2005) From climate change spaghetti to climate change distributions for 21st Century. *San Francisco Estuary and Watershed Science* 3(1)
- Dettinger MD (2011) Climate change, atmospheric rivers and floods in California—A multimodel analysis of storm frequency and magnitude changes: *Journal of American Water Resources Association* 47:514–523
- Dettinger MD, Cayan DR (1995) Large-scale atmospheric forcing of recent trends toward early snowmelt runoff in California. *J Climate* 8:606–623

- Dettinger MD, Cayan DR, Meyer MK, Jeton AE (2004) Simulated hydrologic responses to climate variations and change in the Merced, Carson, and American River basins, Sierra Nevada, California, 1900–2099. *Clim Chang* 62:283–317
- Dettinger M, Hidalgo H, Das T, Cayan D, Knowles N (2009) Projections of potential flood regime changes in California. Public Interest Energy Research, California Energy Commission, Sacramento, CA. Available online at <http://www.energy.ca.gov/2009publications/CEC-500-2009-050/CEC-500-2009-050-D.PDF>
- Dettinger MD, Ralph FM, Hughes M, Das T, Neiman P, Cox D, Estes G, Reynolds D, Hartman R, Cayan D, Jones L (2011) Requirements and designs for a winter storm scenario for emergency preparedness and planning exercises in California. *Natural Hazards*. doi:10.1007/s11069-011-9894-5
- DWR (2005a) Bulletin 160–05 California Water Plan Update
- DWR (2005b) Flood warning: Responding to California's Flood Crisis. State of California, The Resources Agency, Department of Water Resources, January 2005
- DWR (2006) Progress on incorporating climate change into planning and management of California's Water Resources, California Department of Water Resources, Technical Memorandum Report, July 2006
- DWR (2007) A California challenge - flooding in the Central Valley. A report to the Department of Water Resources, State of California, October 2007
- Easterling DR, Meehl GA, Parmesan C, Changnon SA, Karl TR, Mearns LO (2000) Climate extremes: observations, modeling, and impacts. *Science* 288(5487):2068–2074
- Franco G, Cayan D, Moser S, Hanemann M, Jones M-A (2011) Second California Assessment: Integrated Climate Change Impacts Assessment of Natural and Managed Systems. *Climatic Change*. In this Issue
- Griffis VW, Stedinger JR (2007) Incorporating climate change and variability into bulletin 17B LP3 Model, World Environmental and Water Resources Congress 2007: Restoring Our Natural Habitat, American Society of Civil Engineers, 8
- Hamlet AF, Lettenmaier DP (2005) Production of temporally consistent gridded precipitation and temperature fields for the continental U.S. *J Hydrometeorol* 6:330–336
- Hamlet AF, Lettenmaier DP (2007) Effects of 20th Century warming and climate variability on flood risk in the Western U.S. *Water Resour Res* 43:W06427. doi:10.1029/2006WR005099
- Healey M, Dettinger M, Norgaard R (eds) (2008) The state of Bay-Delta science, 2008: CALFED Science Program, 174 p., <http://science.calwater.ca.gov/publications/sbds.html>.
- Hidalgo HG, Dettinger MD, Cayan DR (2008) Downscaling with constructed analogues: daily precipitation and temperature fields over the United States. California Energy Commission, PIER Energy-Related Environmental Research. CEC-500-2007-123. p. 48. Available online: [www.energy.ca.gov/2007publications/CEC-500-2007-123/CEC-500-2007-123.PDF](http://www.energy.ca.gov/2007publications/CEC-500-2007-123/CEC-500-2007-123.PDF)
- Hidalgo HG, Das T, Dettinger MD, Cayan DR, Pierce DW, Barnett TP, Bala G, Mirin A, Wood AW, Bonfils C, Santer BD, Nozawa T (2009) Detection and attribution of climate change in streamflow timing of the Western United States. *J Clim* 22(13):3838–3855
- Intergovernmental Panel on Climate Change (2007) *Climate Change 2007: The physical science basis. Contribution of working group I to the fourth assessment report of the intergovernmental panel on climate change*. In: Solomon, S., D. Qin, M. Manning, Z. Chen, M. Marquis, K.B. Averyt, M. Tignor and H.L. Miller (eds.). Cambridge University Press, Cambridge, United Kingdom and New York, NY, USA, p 996
- Jain S, Lall U, Mann ME (1999) Seasonality and interannual variations of Northern Hemisphere temperature: Equator-to-pole gradient and ocean–land contrast. *J Clim* 12:1086–1100
- Kimball JS, Running SW, Nemani R (1997) An improved method for estimating surface humidity from daily minimum temperature. *Agric For Meteorol* 85:87–98
- Knowles N, Cayan DR (2004) Elevational dependence of projected hydrologic changes in the San Francisco Estuary and watershed. *Clim Chang* 62(1):319–336
- Knowles N, Dettinger M, Cayan D (2006) Trends in snowfall versus rainfall for the Western United States. *J Clim* 19(18):4545–4559
- Lettenmaier DP, Gan TY (1990) Hydrologic sensitivities of the Sacramento–San Joaquin River Basin, California, to global warming. *Water Resour Res* 26:69–86
- Liang X, Lettenmaier DP, Wood EF, Burges SJ (1994) A simple hydrologically based model of land surface water and energy fluxes for GSMs. *J Geophys Res* 99(D7):14,415–14,428
- Lohmann D, Nolte-Holube R, Raschke E (1996) A large scale horizontal routing model to be coupled to land surface parameterization schemes. *Tellus* 48A:708–721
- Maurer EP (2007) Uncertainty in hydrologic impacts of climate change in the Sierra Nevada, California under two emissions scenarios. *Clim Chang* 82(3–4):309–325. doi:10.1007/s10584-006-9180-9
- Maurer EP, Hidalgo HG (2008) Utility of daily vs. monthly large-scale climate data: an intercomparison of two statistical downscaling methods. *Hydrol Earth Syst Sci* 12:551–563
- Maurer EP, Wood AW, Adam JC, Lettenmaier DP, Nijssen B (2002) A long-term hydrologically-based data set of land surface fluxes and states for the conterminous United States. *J Clim* 15:3237–3251

- Maurer EP, Hidalgo HG, Das T, Dettinger MD, Cayan DR (2010a) The utility of daily large-scale climate data in the assessment of climate change impacts on daily streamflow in California. *Hydrol Earth Syst Sci* 14:1125–1138, 113
- Maurer EP, Brekke LD, Pruitt T (2010b) Contrasting lumped and distributed hydrology models for estimating climate change impacts on California watersheds. *J Am Water Resour Assoc* 46(5):1024–1035. doi:10.1111/j.1752-1688.2010.00473
- McCabe GJ, Clark MP, Hay LE (2007) Rain-on-snow events in the Western United States. *BAMS*, 1–10
- Miller NL, Bashford KE, Strem E (2003) Potential impacts of climate change on California hydrology. *J Amer Water Resources Assoc* 771–784
- Milly PCD, Betancourt J, Falkenmark M, Hirsch RM, Kundzewicz ZW, Lettenmaier DP, Stouffer RJ (2008) Stationarity is dead: whither water management? *Science* 319(5863):573–574
- Mo KC, Chelliah M, Carrera ML, Higgins RW, Ebisuzaki W (2005) Atmospheric moisture transport over the United States and Mexico as evaluated in the NCEP regional reanalysis. *J Hydrometeorol* 6:710–728
- Mote P, Hamlet AF, Clark MP, Lettenmaier DP (2005) Declining mountain snowpack in western North America. *Bull Am Meteorol Soc* 86:39–49
- Neiman PJ, Ralph FM, Wick GA, Lundquist JD, Dettinger MD (2008) Meteorological characteristics and overland precipitation impacts of atmospheric rivers affecting the West Coast of North America based on 8 years of SSM/I. *J Hydrometeorol* 9:22–47
- Nijssen B, O'Donnell GM, Lettenmaier DP, Lohmann D, Wood EF (2001) Predicting the discharge of global rivers. *J Clim* 14:3307–3323
- Pandey GR, Cayan DR, Georgakakos KP (1999) Precipitation structure in the Sierra Nevada of California during winter. *J Geophys Res* 104:12019–12030
- Pielke RA Jr, Downton MW (2000) Precipitation and damaging floods: trends in the United States, 1932–97. *J Clim* 13(20):3625–3637
- Pielke RA Jr, Downton MW, Barnard Miller JZ (2002) Flood damage in the United States, 1926–2000: a reanalysis of national weather service estimates. UCAR, Boulder
- Pierce DW, Barnett TP, Bala G, Mirin A, Wood AW, Bonfils C, Santer BD, Nozawa T (2008) Detection and attribution of streamflow timing changes to climate change in the Western United States. *J Clim* 22:3838–3855
- Pierce DW, Barnett TP, Santer BD, Gleckler PJ (2009) Selecting global climate models for regional climate change studies. *Proc Natl Acad Sci*. doi:10.1073/pnas.0900094106
- Raff DA, Pruitt T, Brekke LD (2009) A framework for assessing flood frequency based on climate projection information. *Hydrol Earth Syst Sci* 13(1–18)
- Ralph FM, Neiman PJ, Wick GA, Gutman SI, Dettinger MD, Cayan DR, White AB (2006) Flooding on California's Russian river: Role of atmospheric rivers. *Geophys Res Lett* 33:L13801. doi:10.1029/2006GL026689
- Roos M (1997) The top ten California floods of the 20th Century. In: CM Isaacs, Tharp VL (eds.) *Proceedings of the Thirteenth Annual Pacific Climate 742 (PACLIM) Workshop*. April 15–18, 1996. Interagency Ecological Program. Technical Report 53. 743 California Department of Water Resources, pp. 9–18
- Roos M (2006) Flood management practice in northern California. *Irrig Drain* 55:S93–S99
- Shabri A (2002) A comparison of plotting formulas for the Pearson Type III distributions. *J Technol* 36 (C):61–74
- Sheffield J, Wood EF (2007) Characteristics of global and regional drought, 1950–2000: analysis of soil moisture data from off-line simulation of the terrestrial hydrologic cycle. *J Geophys Res* 112:D17115. doi:10.1029/2006JD008288
- Sivapalan M, Samuel JM (2009) Transcending limitations of stationarity and the return period: process-based approach to flood estimation and risk assessment. *Hydrol Process* 23:1671–1675. doi:10.1002/hyp.7292
- Stewart IT, Cayan DR, Dettinger MD (2005) Changes toward earlier streamflow timing across Western North America. *J Clim* 18:1136–1155
- Thornton PE, Running SW (1999) An improved algorithm for estimating incident daily solar radiation from measurements of temperature, humidity, and precipitation. *Agric For Meteorol* 93:211–228
- Todini E (1996) The ARNO rainfall-runoff model. *J Hydrol* 175:339–382
- Trenberth KE (1999) Conceptual framework for changes of extremes of the hydrological cycle with climate change. *Clim Chang* 42:327–339
- Wood AW, Lettenmaier DP (2006) A testbed for new seasonal hydrologic forecasting approaches in the western U.S. *Bull Am Meteorol Soc* 87:12. doi:10.1175/BAMS-87-12-1699,1699-1712
- Wood EF, Lettenmaier DP, Zartarian VG (1992) A land-surface hydrology parameterization with subgrid variability for general circulation models. *J Geophys Res* 97:2717–2728